This article was published in International Journal of Hydrogen Energy, 40(8), 3485-3496, 2015
http://dx.doi.org/10.1016/j.ijhydene.2014.11.025

Composite-alumina-carbon molecular sieve membranes prepared from novolac resin and boehmite. Part II: Effect of the carbonization temperature on the gas permeation properties

Margot A. Llosa Tanco [a,b], *David A. Pacheco Tanaka* [a,b,*], *Adelio Mendes* [a,**]

[a] *LEPABE-Faculdade de Engenharia, Universidade do Porto, Rua Dr. Roberto Frias, 4200-465 Porto, Portugal*

[b] *Tecnalia-Parque Tecnologico de San Sebastián, Paseo Mikeletegi 2, E-20009 Donostia, San Sebastian, Spain*

Abstract

The influence of carbonization temperature on the permeation properties and aging of thin (4 μm) supported carbon molecular sieve membranes (c-CMSM), prepared from in house synthesized novolac phenolic resin loaded with boehmite nanoparticles, were studied. Just after membrane carbonization (fresh membrane), high permeance to N_2 and O_2 and low O_2/ N_2 permselectivities were observed; the highest permeations were observed for carbonization end temperatures between 500 ^{o}C and 700 ^{o}C. After leaving the c-CMSM 1 day in the air, a large decrease in the permeation and considerable increase in the permselectivity were observed due to the reduction of the pore size by oxygen chemisorption and water physical adsorption; the permeability to H_2 and H_2/N_2 ideal permselectivity for a mem- brane carbonized at 550 ^{o}C are close to palladium membranes for low temperature (<100 ^{o}C). The effect of the permeation characteristics of the membranes carbonized at various temperatures and the removal of water adsorbed in the pores by heat treatment were studied.

Introduction

The growing demand for efficient and "clean" energy has resulted in an increased global acceptance of the so-called "hydrogen economy" as a potential long-term solution to the growing energy crisis [1]. Hydrogen is used in metallurgical chemical, petrochemical, pharmaceutical and textile industries. Therefore, there is a need for a cost effective and efficient means to separate hydrogen from other gases. At present, H_2 can be separated/purified using one of three major processes or their combination: (i) pressure swing adsorption (PSA), (ii) fractional/cryogenic distillation, or (iii) membrane separation. While PSA and fractional/cryogenic distillation systems are in commercial operation,

they are generally not cost effective and especially the fractional/cryogenic distillation is quite energetically demanding for the separation and purification of H^1. Concerning low energy consumption, possibility for continuous operation, easy operation and economical construction costs, membrane separation is currently the most promising process for H_2 separation/purification [1].

Membranes for gas separation processes require high permeability and selectivity. Moreover, they should have good chemical, thermal and mechanical stability and they should be able to be produced continuously and defect-free. There are several membrane materials for hydrogen separation: metallic (mainly Pd based membranes), polymeric, porous inorganic such as silica, zeolite, oxides (alumina, titania, zirconia), and carbon [2,3]. Palladium-based membranes have high selectivities and permeabilities for hydrogen due to their unique permeation mechanism described by the Sieverts' law [1]. Pure Pd membranes are often damaged by hydrogen embrittlement due to the $\alpha-\beta$ phase transition of palladium hydride which occurs at below the critical temperature (300 ^{o}C) and pressure (2 MPa) [4,5]; embrittlement can be minimized by alloying palladium with Ag, Cu or Au [6e8]. Another challenge to Pd membranes is that the presence of S- containing compounds such as hydrogen sulphide (H_2S), which poison the membrane [9]. Pd-Au alloys have been found to reduce embrittlement and improve resistance to catalytic poisoning and corrosive degradation by S compounds while giving rise to higher hydrogen permeability than pure Pd [10,11]. There is still a lot to improve to resolve the current problems associated with Pd membranes, such as the low permeation of H_2 at low temperatures and reducing the amount of Pd used due to its high price. Pacheco Tanaka et al. [12,13], developed a “pore fill” type membrane, where Pd particles are filled in the nano-size pores of a ceramic (g-Al_2O_3 and or YSZ) layer located under the top surface [12,13]. This type of membranes use a fraction of Pd that in the conventional film membranes, and are more resistant to embrittlement; H_2 permeation of 8×10^{-8} mol m^{-2} s^{-1} Pa^{-1} ^{o}C and 6×10^{-7} mol m^{-2} s^{-1} Pa^{-1} ^{o}C at 50 ^{o}C and 100 ^{o}C respectively, were reported.

In the last three decades, gas separation using polymeric membranes has become widely used for a variety of industrial gas separation applications [14]. Among them several mem- branes for hydrogen separation have been studied. In 1979, Monsanto [15] developed the first commercial asymmetric polysulfone hollow fiber membrane and reported a H_2/N_2 selectivity of 39. Ube Industries in Japan [16] reported a poly- imide membrane with a H_2/N_2 selectivity of 35.4, and Separex [17] studied a membrane of polyimide cellulose acetate and

reported a selectivity of 33. Robeson [18] concluded that for polymeric membranes there is a tradeoff between selectivity and permeability and the best performing membranes form an "upper bound" in a log-log plot of selectivity versus permeability. In the past years, it is becoming apparent that new permeability data show only modest shifts in the empirical H_2/N_2 upper bound. Several polymers had become common for hydrogen gas separation membranes, among them are polysulfones (PSF), polycarbonates, cellulose acetate (CA) [19], poly(-phenyllene oxides) (PPO) [20], aramids and polyimides (PI), being the most studied the polyimide Matrimid®. Since several industrial processes involve operations at severe temperature and pressure conditions, these are the main drawbacks of polymeric membranes for hydrogen separation compared to inorganic membranes [21].

Silica membranes are one of the candidates for hydrogen separation. They are low cost microporous inorganic membranes with a network of pores of approximately 0.5 nm of diameter. Silica membranes show low permeation to H_2 and good H_2/N_2 selectivity in dry conditions at 50-600 ^{o}C; however their stability to water vapor is quite poor, even at room temperature [22-24].

Zeolite membranes are inorganic membranes that have uniform molecular size pores. But the presence of inter- crystal pores with sizes larger than the zeolite pores is the major cause for decline in molecular separation efficiency. Now, research is ongoing to resolve the inter-crystalline diffusion path issue using mixed matrix membranes. Zeolite membranes have shown H_2 permeance ranging from 10^{-7} to $<10^{-8}$ mol m^2 s^{-1} Pa^{-1} with a maximum of H_2/N_2 selectivity of 4.8 between 35 and 125 ^{o}C; to be considered useful for gas separation applications these membranes have to be synthesized without macropore size defects or pinholes [25-27].

Carbon molecular sieve membranes (CMSM) were studied for the separation of hydrogen from gasification gas and purification of methane [28], and recovering of H_2 from the waste gas stream [29]. CMSM are inorganic membranes considered as potential candidates for hydrogen separation because of their high mechanical strength and good thermal stability. CMSM are produced by carbonization of a suitable thermo- setting polymeric precursor under an inert atmosphere or vacuum [30e32]. The control over the molecular dimensions of these micropores and the subsequent molecular sieving properties can be tuned by selecting the precursor material and preparation procedure, pre-treatment of the precursor, carbonization temperature history, and post-treatment of the carbonized membranes. The carbonization of polymers in inert or vacuum atmospheres can be separated

into three processes: (i) annealing at 100-400 ^{o}C, (ii) intermediate heat- ing at 400e500 ^{o}C, and (iii) pyrolysis to form carbon at 500-1000 ^{o}C [33]. The pyrolysis process is governed by some parameters such as the heating rate, the final pyrolysis temperature, the thermal soak time, and the pyrolysis atmosphere [34].

Koresh and Soffer [35] prepared membranes carbonizing cellulose hollow fibers. These authors showed the dependence of permeabilities and selectivities on the carbonization temperature and pressure. Hatori [36] reported permeation data of polyimide (Kapton®) membrane film to H_2 and CO_2. Their data showed that increasing the carbonization temperature the size of the micropores decreases. CMSM derived from the carbonization of cellulosic films have been shown by Grainger and Hägg to perform better than polymeric membranes for hydrogen/methane separation in terms of the Robeson type plot [16,18,37]. Table 1 reviews the permeability to H_2 and H_2/N_2 permselectivities for carbon molecular sieve membranes.

The carbonization end temperature in the preparation of CMSM is generally chosen to be above the decomposition point of the polymer but below the graphitization temperature (550 ^{o}C-1000 ^{o}C). Koresh and Soffer [38] studied carbonization end temperature in the range of 800 ^{o}C and 950 ^{o}C, and found that membranes carbonized at the upper temperature exhibited lower permeabilities but higher permselectivities. Geiszler and Koros [39] studied hollow fiber CMSM derived from 6FDA/BPDAeDAM polyimide precursors and found that increasing the carbonization end temperature from 500 ^{o}C to 800 ^{o}C the permeability decreased but the selectivity increased. Similar trends concerning the permeability and selectivity as a function of carbonization temperature have been obtained for other precursor: Kapton (PMDAeODA pol- yimide) [40], P84 polyimide [41], Matrimid polyimide [42], polypyrrolone [43], BTDAeODA polyimide [44,45], and PFA [46]. Briceño et al. [47] coated TiO_2 macroporous tubes in one step with matrimid and pyrolyzed at 550 ^{o}C-700 ^{o}C under nitrogen. After coating the membrane with a thin film of PDMS to eliminate imperfections and pinholes the authors reported H_2/N_2 selectivities of 4.46 and permeance to H_2 of 9.82×10^{-9} mol m^{-2} s^{-1} Pa^{-1}. High pyrolysis temperatures produce increased crystallinity, increased density, and lower average interplanar spacing in CMSM [42,48-51]. In all, for low temperatures, carbon membranes have the potential for a wide variety of applications associated with the separation and purification of hydrogen gas.

Campo et al. [52] prepared CMSM from cellophane paper using a single pyrolysis step and found that the permeability reached a maximum at 550 ^{o}C,

without compromising the selectivity. The Robeson upper bound was overtaken regarding H_2/N_2 separation with a permselectivity of 390. Our group [53] had prepared supported composite-CMSMs (c- CMSMs) derived from resol-phenolic resin loaded with boehmite nanoparticles in a single dipping-drying- carbonization step of a tubular a-alumina membrane sup- port. After carbonization at 550 ^{o}C a selectivity of 14 for the separation of C_3H_6/C_3H_8 was reported; the addition of silver enhanced the selectivity to 38 [54]. CMSM were also prepared varying the composition of resol and boehmite leading to the formation of c-CMSM with different carbon/Al_2O_3; it was found that membranes with higher carbon/Al_2O_3 ratio showed higher permeabilities and lower selectivities; for H_2 a permeability of 2047 barrer and a selectivity for H_2/N_2 of 65.6 was reported [55]. CMSM prepared from resorcinol-formaldehyde resin loaded with boehmite nanoparticles and carbonized at 550 ^{o}C presented micropores with narrower pore-size distribution and higher selectivities than those carbonized at 500 ^{o}C; a H_2 permeability of 301 barrer and selectivity of H_2/N_2 > 586 was reported [56] surpassing the Robeson upper bound for polymeric membranes. c-CMSMs were also prepared using novolac phenolic resin and boehmite nanoparticles in a single dipping-drying-carbonization step on top of a a-Al_2O_3 tubular membrane support; the decrease in performance of the Al-CMSM due to air exposure (aging by adsorption of water), and the changes in the transport properties of the membranes with different activation temperatures for removing water present in the pores were studied using pure gas permeation [57].

This paper studies the effect of the carbonization end temperature in the preparation of c-CMSM using novolac resin and boehmite coated on a-Al_2O_3 tubular membrane support, and their effect in the permeation properties for hydrogen separation at low temperatures.

These carbon membranes can be used for hydrogen separation from reforming gas, after water gas shift to produce power generation and/or chemical grade hydrogen, at temperatures above 250 ^{o}C and pressures above 13 bar and in the presence of impurities such as H_2S and NH_3 [58]. These membranes can also be used to produce oxygen-enriched streams from air, concentrate methane from biogas and xenon from xenon containing streams.

Experimental

Materials

The novolac resin (phenol formaldehyde resin) used as polymeric precursor was synthesized by the acid-catalyzed phenol-formaldehyde condensation [62] as described elsewhere [57]. Briefly, phenol and oxalic acid were placed in a flask fitted with stirrer and a reflux condenser, when the solution reached 80 ^{o}C formaldehyde was added drop-wise, the resin was washed with hot water and further dried. *N*-methyl- 2-pyrrolydone. (NMP), 99.8% purity was supplied by Sigma-Aldrich. Boehmite (10 wt%) particle size 8e20 nm, was provided by Kawaken Fine Chemicals Co. Ltd. The a-alumina tubular supports were supplied by Inopor. Non-porous alumina tubes were purchased from Omega Engineering. The gases were supplied by Air Liquid (99.999% pure). Other chemicals were of reagent grade.

Preparation of tubular ceramic supports

The ends of porous a-Al_2O_3 supports (length 70 mm, and external diameter of 10 mm) were attached to non-porous Al_2O_3 tubes and sealed with a glass sealant at 1150 ^{o}C. The supports have 200 nm mean pore size, located in the outer part of the tube, an effective length of 50 mm was left in the middle.

Preparation of the carbon molecular sieve membranes

Novolac polymer precursor was dissolved in NMP to prepare a 36 wt% resin solution and stirred thoroughly for 24 h to form a homogenous solution. A coating solution containing 13 wt% of novolac resin, 2.4 wt% of formaldehyde, a 0.6 wt% of ethylenediamine and a 83.2 wt% of NMP was prepared, and heated at 100 ^{o}C for 2 h for polymerization; then, a 0.8 wt% dispersion of boehmite nanoparticles was added. The a-alumina tube was coated with this solution by dip-coating using a vacuum pump. The remaining precursor solution was placed in a Teflon dish to make unsupported composite films used for morphological and pore size distribution characterization. Both supported and unsupported membranes were dried in an oven at 100 ^{o}C overnight. The tubular supported membranes were dried under continuous rotation inside an oven to guaranty thickness uniformity.

The membranes were carbonized in a Termolab tubular oven inside a quartz tube (80 mm diameter and 1.5 m in length), using N_2 at flowing

rate of approximately 150 ml min^{-1}-200 ml min^{-1}. First, the temperature was raised from ambient to 100 ^{o}C at a rate of 1 ^{o}C min^{-1} and held at this temperature for 30 min. Then, the temperature was increased from 100 ^{o}C to the desired end temperature with a heating rate of 1 ^{o}C min^{-1} and a soaking time of 2 h. Finally, the oven was allowed to gradually cool to room temperature prior to the removal of the samples. For "fresh membranes", the permeation was determined as soon as the carbon membranes were taken from the oven. The unsupported films were either crushed into small flakes or milled before morphological characterization. c-CMSM were prepared by carbonization at 450, 500, 550, 600, 650, 700, 750, 800, 850 and 1000 ^{o}C e named CMSMT, where *T* is the carbonization end temperature (i.e. CMSM500 for a carbonization end temperature of 500 ^{o}C). At least three membranes for each temperature were prepared. Immediately after carbonization (exposure to air less than 20 s) permeation experiments were performed; these are named "fresh membranes" e letter F added to the membrane name (i.e. CMSM500-F). After 1 day of exposure to air at room temperature, more gas permeation tests were carried out e named CMSMT-1d (i.e. CMSM500-1d indicates a carbon membrane carbonized at 500 ^{o}C and doing the permeation test after 1 day).

After approximately 5 months in the air, membrane CMSM500 (named CMSM500-5m) was heat treated (activated) at various temperatures (100 ^{o}C, 120 ^{o}C, 140 ^{o}C, 160 ^{o}C, 180 ^{o}C and 200 ^{o}C) under N_2 (heating rate 0.7 ^{o}C min^{-1}, soaking time of 120 min) in order to remove water from the pores. After activation, the membrane was left in the oven to cool under N_2 atmosphere and then permeation experiments (N_2, O_2, He, H_2, CO_2) were carried at various feed pressures (100 kPa-500 kPa) and temperatures (20 ^{o}C-100 ^{o}C); the permeation tests were carried for each activation temperature.

Carbon membranes carbonized at 4 different temperatures after approximately 5 months of aging in air (CMSM500-5m, CMSM550-5m, CMSM600-5m and CMSM650-5m) were activated at 200 ^{o}C under N_2 at a heating rate of 0.7 ^{o}C min^{-1} and soaking time of 120 min. Then, as mentioned before, permeation tests were carried at different pressures and temperatures and for different gases.

Characterization of the carbon molecular sieve membranes

Scanning electron microscopy analysis (SEM)

SEM images of the c-CMSMs were taken using a FEI Quanta 400 FEG/EDAX Genesis X4M microscope with 1.2 nm resolution. The tubular supported c-CMSM were fractured and sputtered with platinum to allow better conductivity for SEM.

Raman analysis

Raman analysis were performed on crushed composite-CMSM films using a Renishaw HP IR 785 spectrometer using a 514 nm green laser (Laser physics 25S-514). The spectra were recorded in the range of 500-2000 cm^{-1}, at beam power between 25 and 100 mW Helium-Neon laser with the laser beam focused to a spot size of the order of 2 mm.

Pore size characterization

The microporosity of the composite-CMSM was assessed from the CO_2 adsorption isotherm at 0 ^{o}C. The equilibrium values were obtained using a gravimetric method set up in a Rubotherm® magnetic suspension balance ($\pm 10^{-5}$ mg precision) as described elsewhere [63]. The samples were regenerated with helium at 70 ^{o}C before the measurement.

Gas permeation measurements

For the permeation tests, a shell-and-tube test bench was used, as described elsewhere [53]. Briefly, the test bench uses a pressure controller (Horiba Stec, model UR-7340) for the feed stream and a soap-bubble-film flow meter (STEC SF-2 and STEC SF-3) to measure the permeate flow rate; the temperature was controlled by placing the system into a splitting oven which has three independent heating zones. The selected gas (N_2, O_2, He, H_2 or CO_2) was introduced into the membrane tube from outer shell and the gas permeated was led to the flow meter; flows at various feed pressure differences (100e500 kPa) and at a given temperature were carried and used to calculate the permeance; the average of the permeance are reported.

Results and discussion

Scanning electron microscopy analysis (SEM)

Fig. 1 shows the microphotograph of the cross-sectional view of a CMSM carbonized at 550 ^{o}C. It can be observed a distinct thin layer of the carbon

membrane that was uniformly coated on top of the α-Al_2O_3 support with about 4 μm thickness.

Raman analysis

Raman spectroscopy has been frequently used for characterizing crystalline, nanocrystalline and amorphous carbons. Raman spectra of graphitic carbons consists of two bands, the *G* (graphitic) band at 1575 cm^{-1} and the *D* (disordered graphitic) band at 1355 cm^{-1} [64]. c-CMSM samples carbonized from 500 to 700 ^{o}C were characterized using Raman spectroscopy e Fig. 2; the spectra were recorded in the range of 500-2000 cm^{-1}. It can be seen the presence of two major characteristic bands. First, the graphite band (*G*-band), generally located at 1575 cm^{-1} corresponding to the sp^2 binding structures caused by the stretching vibrations of the C-C bonds, are shifted towards 1580-1596 cm^{-1}, which is characteristics of the carbon materials with disordered-carbon [65]. Second, the disordered band (*D*-band), located between 1300 and 1400 cm^{-1}, which is usually found in amorphous carbon. ID (intensity of the disordered band) and IG (intensity of the graphite band) ratios were used to deter- mine the ratio between disordered and organized phases of carbon in the CMSM samples [65]. As shown in Table 2, the intensity of the *D*-band increases with the temperature, increasing the disorder, corresponding to an increase in amorphous carbon. The same trend was observed by Evelyn et al.[66] using Raman spectroscopy. The fractional value for the amount of disordered carbon, *f*, which is related to the intensity of bands *D* and *G* according with eq. (1) also evidences the increasing amount of disordered carbon [67] - Table 2.

$$f = \frac{I_D}{I_{D+\ I_G}} \qquad (1)$$

Pore size characterization

The adsorption equilibrium isotherms of CO_2 at 0 ^{o}C exhibit type I behavior for the c-CMSM samples carbonized at four different temperatures. The adsorption equilibrium values were obtained using a Rubotherm® suspension magnetic balance [63]. Fig. 3 plots the adsorption equilibrium isotherms of CO_2 at 0 ^{o}C on c-CMSM crashed flakes, treated at different temperatures (450 ^{o}C, 550 ^{o}C, 650 ^{o}C and 750 ^{o}C).

The adsorption mechanism in micropores is known as micropore filling and has been well described by Dubinin and co-workers [68,69]. Dubinin-Radushkevisch (DR) equation was used to fit the experimental results:

$$\frac{W}{W_0} = \exp\left[-\left(\frac{RT\ln(P_0/P)}{E_0}\right)^2\right] \quad (2)$$

where W refers to the micropore volume filled at pressure P, W_0 is the total micropore volume, E_0 the characteristic energy, P_0 the vapor pressure of the free liquid, R is the gas constant and T is the absolute temperature. DR equation gives a reasonable description of adsorption in micropores when the relation obtained for CO_2 is linear. Another equation was proposed, the Dubinin-Astakhov (DA) [70] equation:

$$\frac{W}{W_0} = \exp\left[-\left(\frac{RT\ln(P_0/P)}{E_0}\right)^n\right] \quad (3)$$

where n is a fitting parameter. The adsorption isotherms of CO_2 on c-CMSM are not linear and, therefore, the micropore volume and the characteristic energy were determined fitting the Dubinin-Astakhov equation to the experimental data. Fig. 4 presents the curve for c-CMSM.

The suitability and the applicability of the DA equation were assessed from Fig. 5; since straight fitting line were obtained the DA equation is suitable for these samples. The slope of the plot is related to the characteristic energy of the micropore and the intercept is related to the micropore volume. Table 3 lists the structural parameters obtained for the studied samples.

To obtain a more detailed knowledge of the porous structure of the c-CMSM, their pore size distribution (PSD) was determined using the structure-based method developed by Nguyen et al. [71,72]. Briefly, the method uses the Langmuir isotherm for all pores of size r, while the heterogeneity of the system is described by the distribution of micropores with different size, given by $f(r)$. This method takes into account the potential energy (E) when a molecule is adsorbed on a flat surface, E_S, and the potential energy when a molecule is adsorbed inside a pore, E_{pore}. A slit like pore configuration is assumed here considering the interaction potential energy between graphite type walls and the probe gas molecule. Additionally this model distinguishes between the gas confined in the pore and the adsorbed state and considers the overall contribution of every pore. Further details about this method can be found elsewhere [71,73]. The pore size distribution for c-CMSM carbonized at 450, 550, 650 and 750 ^{o}C were obtained and are presented in Figs. 5 and 6.

It can be seen from Figs. 5 and 6 that the c-CMSM samples show both the presence of small micropores (0.3 nm-0.7 nm range) and larger micropores (0.7 nm-1 nm). Sample CMSM- 450 has a small volume of pores with pores ranging from 0.4 nm to 0.9 nm and sample CMSM-550 has a significant higher pore volume and pores ranging from 0.45 nm to 0.8 nm; sample CMSM-650 shows a higher pore volume and a bidisperse pore size distribution with a significantly larger volume of small micropores (0.35 nm-0.45 nm); finally sample CMSM- 750 exhibits a smaller volume of small micropores (0.35 nm-0.45 nm) and a larger volume of intermediate size micropores (0.5-0.8 nm) with a very defined pore size distribution of pores ranging between 0.35 nm and 0.45 nm normally assigned to the permselectivity behavior of the membrane. These results show that as the carbonization temperature increases the volume and the number of smaller micropores increases up to 650 ^{o}C. This will influence the permeability and permselectivity performance of the carbon membranes, as it will be shown below. The results are consistent with the PSD found for c-CMSM derived from the resol resin [53] showing both small and larger micropores (0.35-0.45 nm and 0.5-0.8 nm). The pore size distribution determined is also consistent with the permeation results shown in Table 4 where the permeability increases from CMSM-450 to CMSM-650 correlating well with the increase of the pore volume and the selectivity increases for sample CMSM-750 where pore constrictions volume pores ranging between 0.35 nm and 0.45 nm is well defined.

Permeation experiments

Effect of carbonization end temperature on the permeation of "fresh membranes" The permeance of the supported carbon membranes obtained from 450 ^{o}C to 1000 ^{o}C was evaluated for N_2 (0.364 nm [74]), and O_2 (0.346 nm [74]) e the values in brackets correspond to the kinetic diameter of the gases. Permeation experiments were carried at room temperature just after the membrane carbonization (fresh membranes) to prevent the adsorption of water; the exposure to air was less than 20 s. The duration of each permeation test was ca. 2 h, the gas permeation measurements were made until readings stabilize. Throughout the various test phases, membrane performance was periodically evaluated using pure gas permeation tests (with He or N_2). The permeances and ideal permselectivities for the fresh carbon membranes are summarized in Table 4 and the effect of carbonization end temperature on the permeances to N_2 and O_2 are shown in Fig. 7. For both gases all membranes showed high permeances, though small selectivities; from 450 ^{o}C, the permeation increases as the

carbonization end temperature increases peaking between 500 ^{o}C and 700 ^{o}C. These results show that the permeation depends on the carbonization end temperature; at 450 ^{o}C few pores are formed and as the temperature increases more functional groups are removed producing more pores; from 650 ^{o}C condensation reactions are predominant therefore smaller pores are formed decreasing the gas permeation. These results are consistent with the pore size distribution shown in Figs. 5 and 6 where it was seen that as the carbonization temperature increases the volume and the number of smaller micropores up to 650 ^{o}C, and for the sample carbonized at 750 ^{o}C the selectivity increases.

Effect of carbonization end temperature on the permeation of "aged membranes" (1 day).

The fresh membranes were left in the laboratory bench at room temperature for 1 day. Then the permeance and selectivities of the c-CMSM samples to O_2, N_2, He and H_2 were obtained (Table 5). Compared with fresh membranes (Table 4), the permeances decreased more markedly for N_2 (700 times for N_2 and 66 times for O_2); samples carbonized at temperatures above 600 ^{o}C showed permeance out of the range of the flow-meter used. The decrease of permeation after 1 day should be related to the reaction of reactive groups presented in the fresh membrane with water producing functional groups containing oxygen (chemisorption), making the pores smaller and hydrophilic, able to adsorb water ([75e78] physisorption). O_2/N_2 permselectivity increases with the temperature; for the membrane calcinated at 550 ^{o}C this value was 15. Permselectivities for higher carbonization end temperatures were not possible to measure.

Since H_2 and He are smaller, permeance studies for these two gases were carried out and their relation with the temperature of carbonization is shown in Fig. 8 and Table 5; highest permeance are observed for samples carbonized at 500 and 550 ^{o}C. These carbon membranes show higher permeance for H_2 than for He despite of H_2 being larger than helium (0.29 and 0.26 nm for H_2 and He, respectively) [74]; this was attributed to the larger adsorption affinity of H_2 [40] and to the cross-section diameter of H_2, which is smaller. In Fig 9 the revised Robeson upper bound line for H_2/N_2 separation, including some representative state of the art membrane values [77], and the experimental values obtained in the pre- sent work, are presented. Sample CMSM550-1d (C1) is located above the upper bound line and is located between the performances of Pd pore filled membranes at 100 ^{o}C (Pd1) and at 50 ^{o}C (Pd2) [12]. The Pd membrane

permeation to hydrogen decreases with the temperature; below 100 ^{o}C it is low and membranes are sensitive to embrittlement. Pore filled type membranes, however, are more resistant towards embrittlement and therefore these values were used as comparison.

Since CMSM are: a) cheaper, b) embrittlement free, and c) resistant to sulfur or carbon monoxide poisoning, they are more suitable for hydrogen separation at low temperatures.

Permeation studies of membrane carbonized at 500 ^{o}C after 5 months of aging.

Since the aged membranes have low gas permeation due to the water presence in the pores, the effect of removing that water by heating (activation) was studied. The c-CMSM sample carbonized at 500 ^{o}C and aged for approximately 5 months (c-CMSM500-5m) was activated under N_2 flow at 200 ^{o}C, with a heating rate of 0.7 ^{o}C/min and soaking time of 120 min. Permeation tests were performed with N_2, O_2, He, H_2 and CO_2 and at different permeation temperatures (from 40 ^{o}C to 120 ^{o}C) and at different feed pressure (from 100 kPa to 500 kPa). The permeance values obtained are given in Fig. 10. Similar permeation tests were carried for c-CMSM500-5m sample activated at 100 ^{o}C, 120 ^{o}C, 140 ^{o}C, 160 ^{o}C, 180 ^{o}C, and 200 ^{o}C; the permeance values for each pressure were calculated and the average of these values are listed in Supplementary information S1.

Fig. 11 shows the Arrhenius plot for the membrane activated at 120 ^{o}C. From the data of permeance at different temperatures of the activated c-CMSM-500-5m (S1), the activation energy (E_a) was calculated.

$$\mathrm{Ln}\, J = \frac{E_a}{R}\left(\frac{1}{T}\right) + c \qquad (4)$$

The values of E_a of c-CMSM-500-5m for N_2, O_2, He, H_2 and CO_2 are listed in Table 6 and illustrated in Fig. 12.

Fig. 12, shows that a) for all gases E_a increases with the permeant size; for bulkier molecules the energy needed to pass through the pores is higher; b) E_a decreases as the temperature of carbonization of the membrane increases; c) for CO_2, at temperatures lower than 200 ^{o}C, E_a values are higher than bulkier species N_2 and O_2. The permeation behavior of CO_2 should be related to the fact of CO_2 presenting a high adsorption affinity towards CMSMs. Assuming sorption- diffusion transport mechanism, since CO_2 adsorption is lower at higher temperatures makes the CO_2 transport in these conditions less favorable

(Fig 12).

Permeation studies of the membranes carbonized at various temperatures and heated at 200 ^{o}C

Carbon membranes c-CMSM500-5m, c-CMSM550-5m, c- CMSM600-5m and c-CMSM650-5m were activated under N_2 at 200 ^{o}C, with a heating rate of 0.7 ^{o}C min^{-1}, for 120 min. The permeation to N_2, O_2, CO_2, H_2 and He were obtained and results are listed in the Supplementary information S2. From these values, E_a were calculated using eq. (4) and the results are listed in Table 7 and illustrated in Fig 13.

E_a increases with the kinetic diameter of the gases for c- CMSM carbonized at more than 600 ^{o}C. It is more difficult for N_2 to permeate because pores became smaller. Membranes carbonized at more than 650 ^{o}C show too small permeances to N_2, O_2, and CO_2 to be detected and only the permeance to fast species H_2 and He were measured. H_2 has higher E_a than H_2 which increases as the carbonization temperature increases; another indication that the pore size decreases with the temperature. E_a for CO_2 in membranes activated at 200 ^{o}C are in line with its size (see Fig. 13).

Fig. 14 presents the revised Robeson upper bound line [77] for H_2/CO_2 including values from the literature and from this work. It can be seen that CMSM600 membrane activated at 200 ^{o}C and characterized at 30 ^{o}C (CMSM600-30) exceeds the upper bound.

Conclusions

Thin composite alumina CMS membranes were successfully fabricated by carbonizing novolac phenolic resin coated on α-alumina tubular membranes using a single dip step. It was concluded that the carbonization end temperature was important for the permeation characteristics of the membranes; the pore size decreases with the carbonization temperature within 450 ^{o}C-1000 ^{o}C temperature range.

Membrane samples just after carbonization show high gas permeation that decreases quickly upon contacting with room atmosphere; this behavior was assigned to the water physical and chemical adsorption on the pore network. After 1 day contacting with the atmospheric air, the membrane carbonized at 550 ^{o}C showed an O_2/N_2 selectivity of 15 at room temperature and performs above

the Robeson upper bound; the H_2/N_2 selectivity was 725 and the permeance to H_2 was 145 $\times$ 10^{-9} mol m^{-2} s^{-1} Pa^{-1} at room temperature, values comparable with the best performing to Pd membranes. This CMS membrane can therefore be used instead of Pd for H_2 separation processes involving hydrogen membranes at low temperature. The gas permeation of aged membranes can be increased heating them from 100 ^{o}C to 200 ^{o}C; this enhancement was assigned to the removal of physically adsorbed water. From the gas permeation at different feed pressures and temperatures, it was possible to calculate the permeation activation energy, E_a for N_2, O_2, CO_2, He and H_2; the permeation increases as the water is removed and the E_a increases with the size of the permeant species; below 200 ^{o}C, CO_2 has a higher activation energy than expected according to its size, this due to the permeation mechanism of molecular sieving and adsorption

Acknowledgments

Margot Llosa Tanco is grateful to the Portuguese Foundation for Science and Technology (FCT) for her doctoral grant (reference SFRH/BD/61898/2009). The authors would like to acknowledge to Sandra C. Rodrigues (doctoral grant reference SFRH/BD/90208/2012) for performing the CO_2 adsorption measurements at LEPABE and FCT research project PTDC/ EQU-EQU/114944/2009. The authors are also thankful to CEMUP for the SEM analysis (REEQ/1062/CTM/2005 and REDE/ 1512/RME/2005 funding provided by FCT).

Appendix A. Supplementary data

Supplementary data related to this article can be found at http://dx.doi.org/10.1016/j.ijhydene.2014.11.025.

References

1. Ockwig NW, Nenoff TM. Membranes for hydrogen separation. Chem Rev Oct. 2007;107(10):4078-110.
2. Basile Angelo, Gallucci Fausto. Membranes for membrane Reactors: preparation, optimization and selection. John Wiley Sons, Ltd. Publ; 2011.
3. Lin YS. Microporous and dense inorganic membranes: current status and prospective. Sep Purif Technol Oct. 2001;25(1e3):39-55.

4. Paglieri SN, Way JD. “Innovations in palladium membrane research. Sep Purif Rev Jul. 2002;31(1):1-169.
5. Roa F, Block MJ, Way JD. The influence of alloy composition on the H2 flux of composite Pd Cu membranes. Desalination Sep. 2002;147(1-3):411-6.
6. Pacheco Tanaka DA, Llosa Tanco MA, Niwa S, Wakui Y, Mizukami F, Namba T, et al. Preparation of palladium and silver alloy membrane on a porous a-alumina tube via simultaneous electroless plating. J Memb Sci Feb. 2005;247(1e2):21-7.
7. Okazaki J, Pacheco Tanaka DA, Llosa Tanco MA, Wakui Y, Mizukami F, Suzuki TM. Hydrogen permeability study of the thin Pd-Ag alloy membranes in the temperature range across the α–β phase transition. J Memb Sci Oct. 2006;282(1-2):370-4.
8. Okazaki J, Ikeda T, Pacheco Tanaka DA, Sato K, Suzuki TM, Mizukami F. An investigation of thermal stability of thin palladium-silver alloy membranes for high temperature hydrogen separation. J Memb Sci Jan. 2011;366(1-2):212-9.
9. C, T, F J, Gabitto. Sulfur poisoning of metal membranes for H2 separation. 2009.
10. Ma YH, Mardilovich IP, Engwall EE. Thin composite palladium and palladium/alloy membranes for hydrogen separation. Ann N Y Acad Sci Mar. 2003;984(1):346-60.
11. Yun S, Ted Oyama S. Correlations in palladium membranes for hydrogen separation: a review. J Memb Sci Jun. 2011;375(1-2):28-45.
12. Pacheco Tanaka DA, Llosa Tanco MA, Nagase T, Okazaki J, Wakui Y, Mizukami F, et al. Fabrication of hydrogen- permeable composite membranes packed with palladium nanoparticles. Adv Mater Mar. 2006;18(5):630-2.
13. Pacheco Tanaka DA, Llosa Tanco MA, Okazaki J, Wakui Y, Mizukami F, Suzuki TM. Preparation of ‘pore-fill’ type PdeYSZeg-Al2O3 composite membrane supported on α- Al2O3 tube for hydrogen separation. J Memb Sci Jul. 2008;320(1-2):436-41.
14. Sanders DF, Smith ZP, Guo R, Robeson LM, McGrath JE, Paul DR, et al. Energy-efficient polymeric gas separation membranes for a sustainable future: a review. Polym Guildf Aug. 2013;54(18):4729-61.
15. Henis, Tripodi. Multicomponent membranes for gas separations. 4230463. 1980.
16. Grainger D, Hagg M. The recovery by carbon molecular sieve membranes of hydrogen transmitted in natural gas networks. Int J Hydrogen Energy May 2008;33(9):2379-88.
17. Schell W, Houston C. Spiral-wound permeators for purification and recovery. Chem Eng Prog 1982;78(10):33-7.

18. Robeson LM. Correlation of separation factor versus permeability for polymeric membranes. J Memb Sci Oct. 1991;62(2):165-85.
19. Puleo AC, Paul DR, Kelley SS. The effect of degree of acetylation on gas sorption and transport behavior in cellulose acetate. J Memb Sci Dec. 1989;47(3):301-32.
20. Koros WJ, Fleming GK, Jordan SM, Kim TH, Hoehn HH. Polymeric membrane materials for solution-diffusion based permeation separations. Prog Polym Sci Jan. 1988;13(4):339-401.
21. Hosseini SS, Teoh MM, Chung TS. Hydrogen separation and purification in membranes of miscible polymer blends with interpenetration networks. Polym Guildf Mar. 2008;49(6):1594-603.
22. Morooka S, Kusakabe K. Microporous inorganic membranes for gas separation. MRS Bull Mar. 1999;24(03):25-9.
23. Prabhu AK, Oyama ST. Highly hydrogen selective ceramic membranes: application to the transformation of greenhouse gases. J Memb Sci Aug. 2000;176(2):233-48.
24. Verweij H. Ceramic membranes: morphology and transport. J Mater Sci Dec. 2003;38(23):4677-95.
25. Nomura M, Yamaguchi T, Nakao S. Silicalite membranes modified by counter diffusion CVD technique. Ind Eng Chem Res Oct. 1997;36(10):4217-23.
26. Pechar T, Kim S, Vaughan B, Marand E, Tsapatsis M, Jeong H, et al. Fabrication and characterization of polyimideezeolite L mixed matrix membranes for gas separations. J Memb Sci Jun. 2006;277(1-2):195-202.
27. Husain S, Koros WJ. Mixed matrix hollow fiber membranes made with modified HSSZ-13 zeolite in polyetherimide polymer matrix for gas separation. J Memb Sci Feb. 2007;288(1-2):195-207.
28. Fuertes A, Centeno T. Preparation of supported carbon molecular sieve membranes. Carbon N Y Mar. 1999;37(4):679-84.
29. Rao MB, Sircar S. Nanoporous carbon membranes for separation of gas mixtures by selective surface flow. J Memb Sci Dec. 1993;85(3):253-64.
30. Saufi S. Fabrication of carbon membranes for gas separationeea review. Carbon N. Y 2004;42(2):241-59.
31. Salleh WNW, Ismail AF. Effects of carbonization heating rate on CO2 separation of derived carbon membranes. Sep Purif Technol Mar. 2012;88:174-83.
32. Ismail A, David L. A review on the latest development of carbon membranes for gas separation. J Memb Sci Oct. 2001;193(1):1-18.
33. Barsema J, Klijnstra S, Balster J, Vandervegt N, Koops G, Wessling M. Intermediate polymer to carbon gas separation membranes based on matrimid

PI. J Memb Sci Jul. 2004;238(1-2):93-102.
34. F HC, Ismail AF, Rana D, Matsuura T. Carbon-based membranes for separation processes. Springer; 2011.
35. Koresh JE, Soffer A. The carbon molecular sieve membranes. General properties and the permeability of CH4/H2 mixture. Sep Sci Technol Feb. 1987;22(2-3):973-82.
36. Hatori H, Takagi H, Yamada Y. Gas separation properties of molecular sieving carbon membranes with nanopore channels. Carbon N. Y Jan. 2004;42(5-6):1169-73.
37. Grainger D, Hägg M-B. Evaluation of cellulose-derived carbon molecular sieve membranes for hydrogen separation from light hydrocarbons. J Memb Sci Dec. 2007;306(1-2):307-17.
38. Koresh J, Soffer A. 185. A molecular sieve carbon membrane for continuous process gas separation. Carbon N. Y Jan. 1984;22(2):225.
39. Geiszler VC, Koros WJ. Effects of polyimide pyrolysis conditions on carbon molecular sieve membrane properties. Ind Eng Chem Res 1996;35(9):2999-3003.
40. Suda H, Haraya K. Gas permeation through micropores of carbon molecular sieve membranes derived from kapton polyimide. J Phys Chem B 1997;101(96):3988-94.
41. Tin PS, Chung T-S, Liu Y, Wang R. Separation of CO2/CH4 through carbon molecular sieve membranes derived from P84 polyimide. Carbon N Y Jan. 2004;42(15):3123-31.
42. Xiao Y, Dai Y, Chung T-S, Guiver MD. Effects of brominating matrimid polyimide on the physical and gas transport properties of derived carbon membranes. Macromolecules 2005;38(24):10042-9.
43. Kita H, Yoshino M, Tanaka K, Okamoto K. Gas permselectivity of carbonized polypyrrolone membrane. Chem Commun Jan. 1997;(11):1051-2.
44. Kim Y, Park H, Lee Y. Preparation and characterization of carbon molecular sieve membranes derived from BTDAeODA polyimide and their gas separation properties. J Memb Sci Jun. 2005;255(1-2):265-73.
45. Park H. Relationship between chemical structure of aromatic polyimides and gas permeation properties of their carbon molecular sieve membranes. J Memb Sci Feb. 2004;229(1-2):117-27.
46. Barsema J, Balster J, Jordan V, van der Vegt NF, Wessling M. Functionalized carbon molecular sieve membranes containing Ag-nanoclusters. J Memb Sci Jul. 2003;219(1-2):47-57.
47. Bricen̜o K, Montane D, Garcia-Valls R, Iulianelli A, Basile A. Fabrication variables affecting the structure and properties of supported carbon molecular sieve membranes for hydrogen separation. J Memb Sci Oct. 2012;415-416:288-97.

48. Anderson C, Pas S, Arora G, Kentish S, Hill A, Sandler S, et al. Effect of pyrolysis temperature and operating temperature on the performance of nanoporous carbon membranes. J Memb Sci Sep. 2008;322(1):19-27.
49. Song C, Wang T, Wang X, Qiu J, Cao Y. Preparation and gas separation properties of poly(furfuryl alcohol)-based C/CMS composite membranes. Sep Purif Technol Jan. 2008;58(3):412-8.
50. Lua AC, Su J. Effects of carbonisation on pore evolution and gas permeation properties of carbon membranes from Kapton® polyimide. Carbon N Y Nov. 2006;44(14):2964-72.
51. Suda H, Haraya K. Molecular sieving effect of carbonized kapton polyimide membrane. J Chem Soc Chem Commun Jan. 1995;(11):1179.
52. Campo MC, Magalhães FD, Mendes A. Carbon molecular sieve membranes from cellophane paper. J Memb Sci Mar. 2010;350(1-2):180-8.
53. Teixeira M, Campo MC, Pacheco Tanaka DA, Llosa Tanco MA, Magen C, Mendes A. Composite phenolic resin-based carbon molecular sieve membranes for gas separation. Carbon N Y Nov. 2011;49(13):4348-58.
54. Teixeira M, Campo M, Pacheco Tanaka DA, Llosa Tanco MA, Magen C, Mendes A. CarboneAl2O3eAg composite molecular sieve membranes for gas separation. Chem Eng Res Des Dec. 2012;90(12):2338-45.
55. Teixeira M, Rodrigues SC, Campo M, Pacheco Tanaka DA, Llosa Tanco MA, Madeira L, et al. Boehmite-phenolic resin carbon molecular sieve membranes-permeation and adsorption studies. Chem Eng Res Des 2014;92:2668-80.
56. Rodrigues SC, Whitley R, Mendes A. Preparation and characterization of carbon molecular sieve membranes based on resorcinol-formaldehyde resin. J Memb Sci Jun. 2014;459:207-16.
57. Llosa Tanco MA, Pacheco Tanaka DA, Rodrigues SC, Texeira M, and Mendes A, "Composite-alumina-carbon molecular sieve membranes prepared from novolac resin and boehmite. Part I: preparation, characterization and gas permeation studies."
58. Parsley D, Ciora R, Flowers D, Laukaitaus J, Chen A, Liu P, et al. Field evaluation of carbon molecular sieve membranes for the separation and purification of hydrogen from coal- and biomass-derived syngas. J Memb Sci Jan. 2014;450:81-92.
59. Suda H, Haraya K. Gas permeation through micropores of carbon molecular sieve membranes derived from kapton polyimide. J Phys Chem B May 1997;101(20):3988-94.
60. Shiflett MB. Ultrasonic deposition of high-selectivity nanoporous carbon membranes. Science Sep. 1999;285(5435):1902-5.
61. Hosseini SS, Chung TS. Carbon membranes from blends of PBI and

polyimides for N2/CH4 and CO2/CH4 separation and hydrogen purification. J Memb Sci Feb. 2009;328(1-2):174-85.
62. Braun. Polymer synthesis theory and practice fundamentals methods experiments. 4th ed. Springer; 2012.
63. Campo MC, Magalhães FD, Mendes A. Comparative study between a CMS membrane and a CMS adsorbent: Part I-morphology, adsorption equilibrium and kinetics. J Memb Sci Jan. 2010;346(1):15-25.
64. Sadezky A, Muckenhuber H, Grothe H, Niessner R, Pöschl U. Raman microspectroscopy of soot and related carbonaceous materials: spectral analysis and structural information. Carbon N. Y Jul. 2005;43(8):1731-42.
65. Supova M, Svitilova J, Chlup Z, Cerny M, Weishauptova Z. Relation between mechanical properties and pyrolysis temperature of phenol formaldehyde resin for gas separation membranes 2012;56(1):40-9.
66. Evelyn AL, Ila D, Jenkins GM. RBS and Raman spectroscopy study of heat-treatment effect on phenolformaldehyde resin. Nucl Instrum Methods Phys Res Sect B Beam Interact Mater Atoms Mar. 1994;85(1-4):861-3.
67. Kishore N, Sachan S, Rai KN, Kumar A. Synthesis and characterization of a nanofiltration carbon membrane derived from phenol e formaldehyde resin 2003;41:2961-72.
68. Xiao Y, Chng M, Chung T, Toriida M, Tamai S, Chen H, et al. Asymmetric structure and enhanced gas separation performance induced by in situ growth of silver nanoparticles in carbon membranes. Carbon N Y Feb. 2010;48(2):408-16.
69. Ottaway M. Use of thermogravimetry for proximate analysis of coals and cokes. Fuel Aug. 1982;61(8):713-6.
70. Gil A, Korili SA, Cherkashinin GY. Extension of the Dubinine Astakhov equation for evaluating the micropore size distribution of a modified carbon molecular sieve. J Colloid Interface Sci Jul. 2003;262(2):603-7.
71. Nguyen C, Do DD. Adsorption of supercritical gases in porous media: determination of micropore size distribution. J Phys Chem B Aug. 1999;103(33):6900-8.
72. Nguyen C, Do DD, Haraya K, Wang K. The structural characterization of carbon molecular sieve membrane (CMSM) via gas adsorption. J Memb Sci Aug. 2003;220(1-2):177-82.
73. Rutherford SW, Do DD. Characterization of carbon molecular sieve 3A. Langmuir Sep. 2000;16(18):7245-54.
74. Breck DW. Zeolite molecular sieves, structure, chemistry and use. New York: John Wiley & Sons Ltd.; 1974.
75. Campo MC, Lagorsse S, Magalhães FD, Mendes A. Comparative study between a CMS membrane and a CMS adsorbent: part II. Water vapor

adsorption and surface chemistry. J Memb Sci Jan. 2010;346(1):26-36.
76. Rutherford SW. Modeling water adsorption in carbon micropores: study of water in carbon molecular sieves. Langmuir Jan. 2006;22(2):702-8.
77. Robeson LM. The upper bound revisited. J Memb Sci Jul. 2008;320(1-2):390-400.
78. Tseng H-H, Itta AK. Modification of carbon molecular sieve membrane structure by self-assisted deposition carbon segment for gas separation. J Memb Sci Feb. 2012;389:223-33.
79. Zhou W, Yoshino M, Kita H, Okamoto K. "Preparation and gas permeation properties of carbon molecular sieve membranes based on sulfonated phenolic resin. J Memb Sci Jun. 2003;217(1-2):55-67.
80. Low BT, Xiao Y, Chung TS, Liu Y. Simultaneous occurrence of chemical grafting, cross-linking, and etching on the surface of polyimide membranes and their impact on H2/CO2 separation. Macromolecules Feb. 2008;41(4):1297-309.
81. Bux H, Liang F, Li Y, Cravillon J, Wiebcke M, Caro J. Zeolitic imidazolate framework membrane with molecular sieving properties by microwave-assisted solvothermal synthesis. J Am Chem Soc Nov. 2009;131(44):16000-1.
82. McCarthy MC, Varela-Guerrero V, V Barnett G, Jeong H-K. Synthesis of zeolitic imidazolate framework films and membranes with controlled microstructures. Langmuir Sep. 2010;26(18):14636-41.

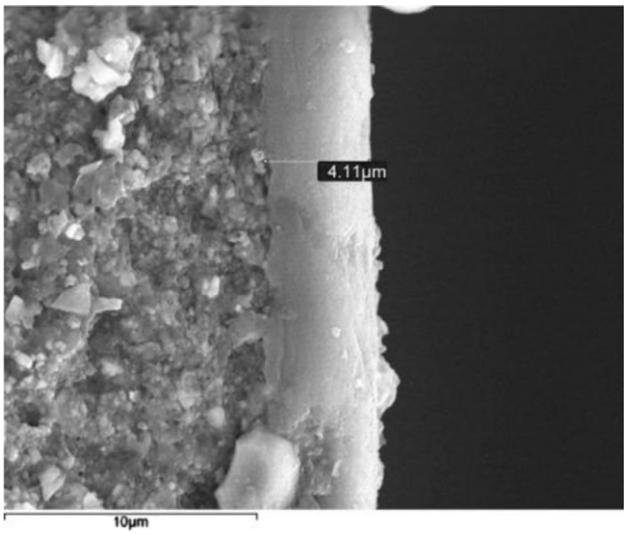

Fig. 1 - SEM photograph of the cross-section region of the c-CMSM supported on the alumina tube.

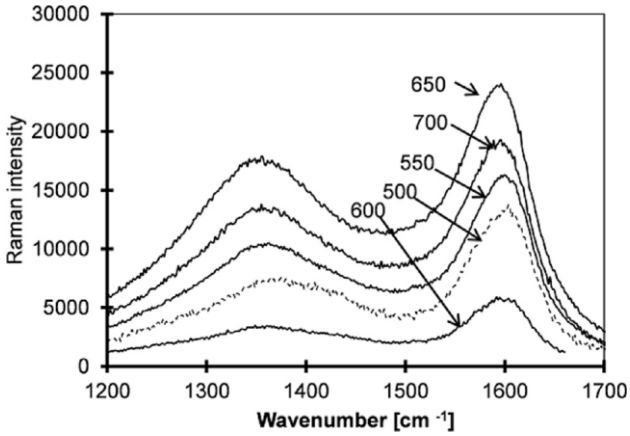

Fig. 2 -Raman spectra for c-CMSM carbonized at various end temperatures.

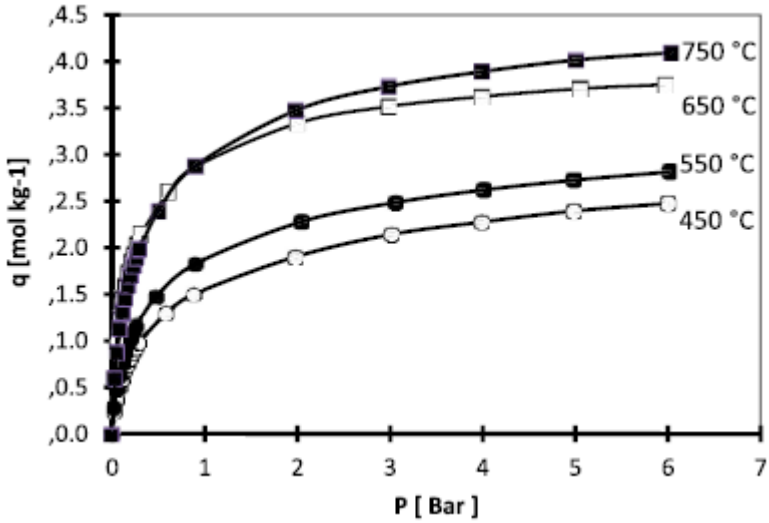

Fig. 3 - Adsorption equilibrium isotherm of CO2 at 0 ºC on the c-CMSM samples carbonized at 450, 550, 650 and 750 ºC

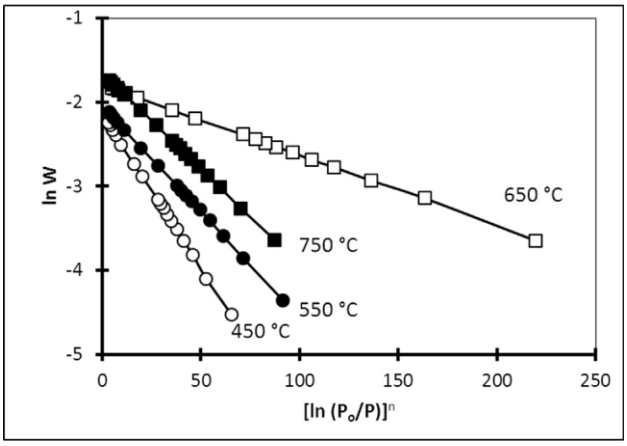

Fig. 4 - Carbon dioxide characteristic curve for the c-CMSM carbonized at 450, 550, 650 and 750 ºC.

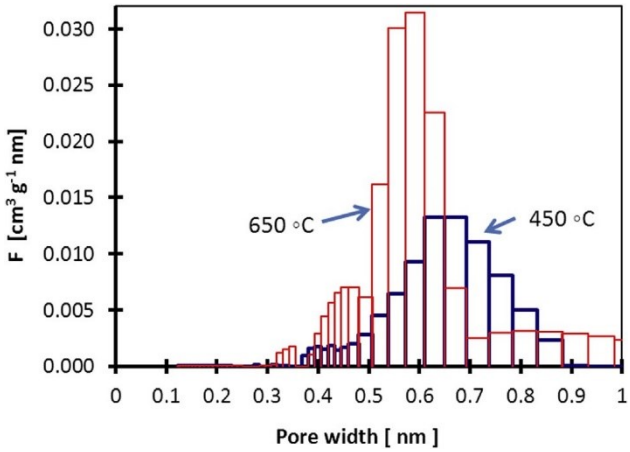

Fig. 5 - Micropore size distribution of c-CMSM carbonized at 450 and 650 ^{O}C.

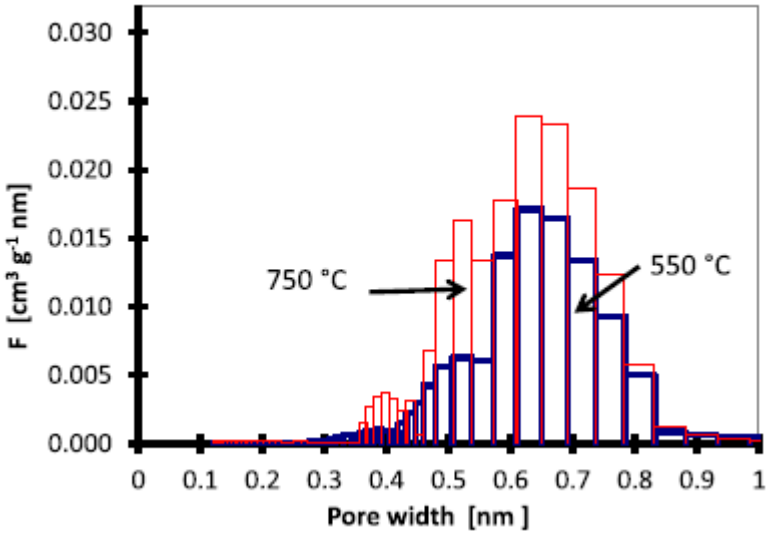

Fig. 6 - Micropore size distribution of c-CMSM carbonized at 550 and 750 ^{O}C.

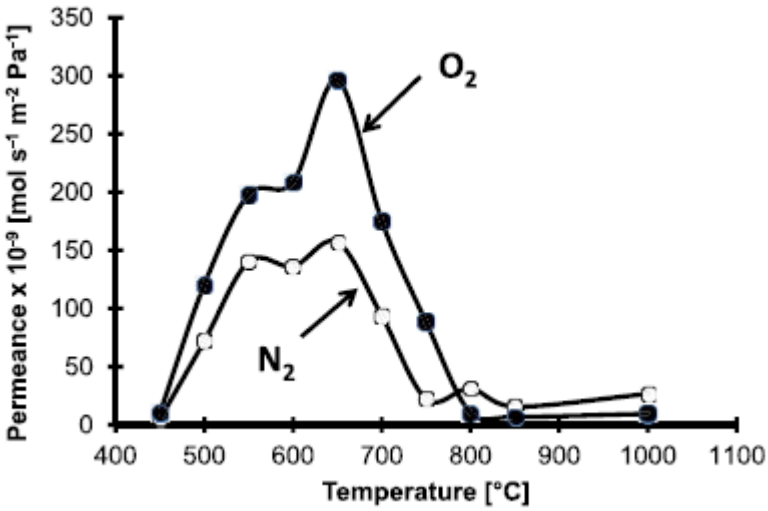

Fig. 7 - c-CMSM permeance to N2 and O2 as a function of carbonization end temperature

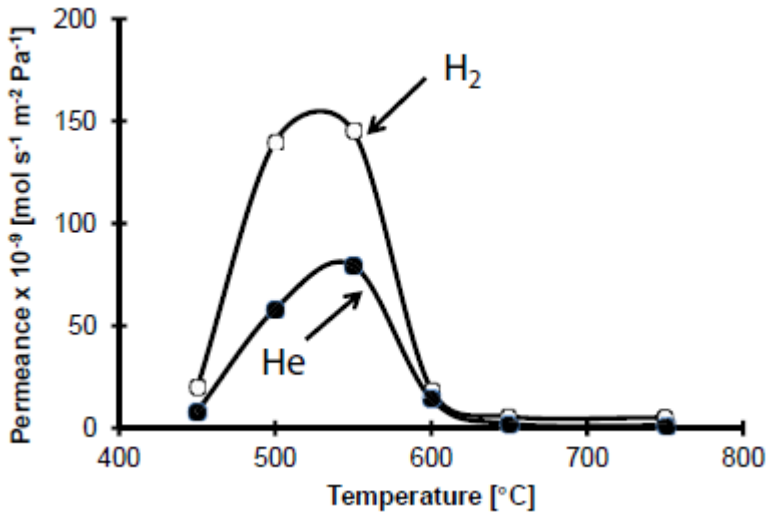

Fig. 8 - Permeance of c-CMSM carbonized at various temperatures and after 1 day aging to He and H2 (lines were added for readability).

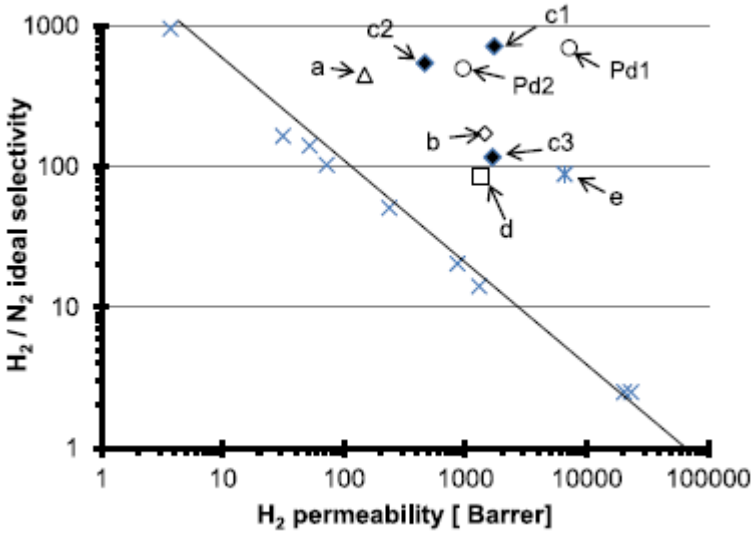

Fig. 9 - Robeson upper bound plot for H2/N2 for: (a) Campo [52], (b) Tseng [78], (c1) This work (CMSM550-1d); (c2) This work (CMSM600-5m); (c3) This work (CMSM500-1d); (d) Hosseini [61], (e) Kita [79](Pd1) Pd pore filled membranes at 100 ^{o}C; and (Pd2) Pd pore filled membranes at 50 ^{o}C [12].

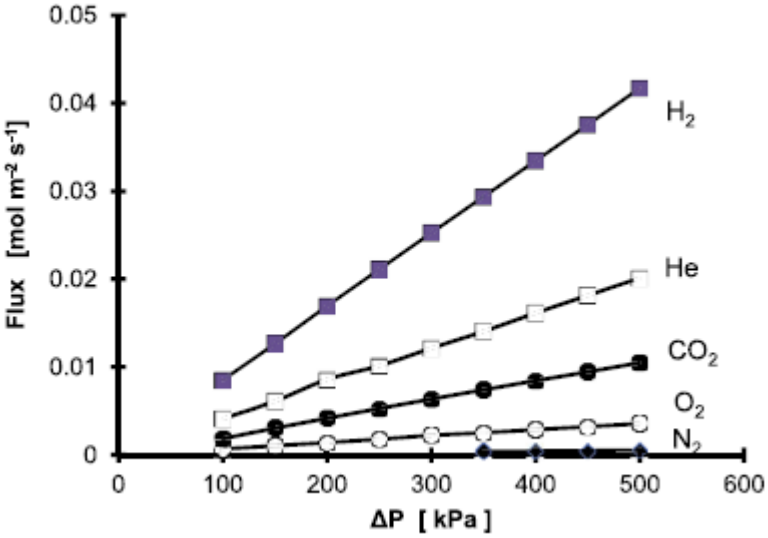

Fig. 10 - Permeation fluxes through membrane c-CMSM- 500-5m (activated at 200 ^{o}C) as a function of the relative feed pressure at 60 ^{o}C and for different single gases

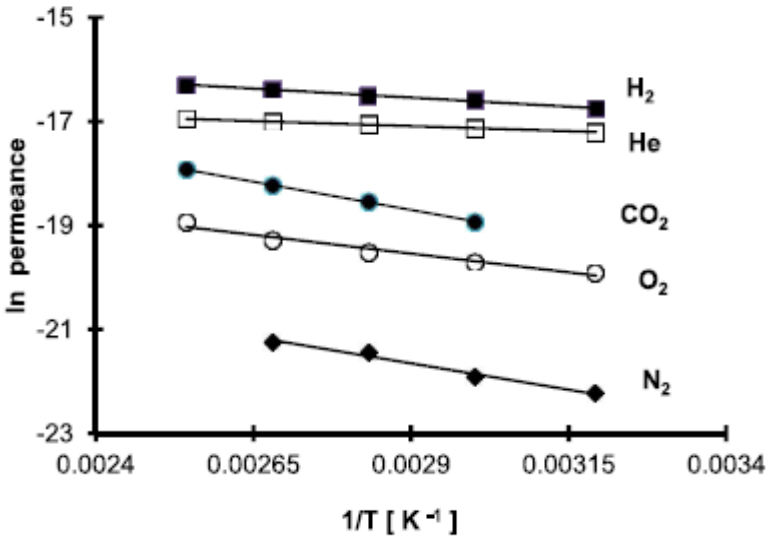

Fig. 11 - Arrhenius type plot of permeance for various gases measured at room temperature of aged membrane c- CMSM-500-5m activated at 120 ^{o}C.

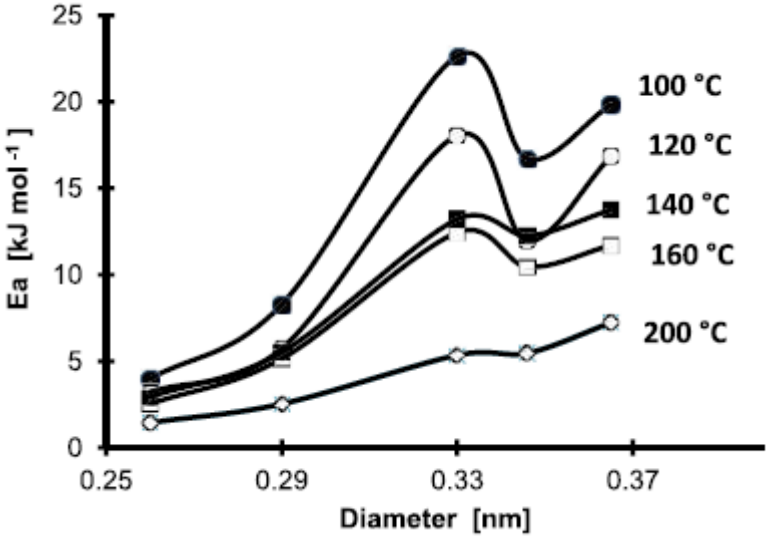

Fig. 12 - Activation energy in c-CMSM-500 membrane activated from 100 to 200 ^{o}C, for: N2 (0.365 nm), O2 (0.346 nm), CO2 (0.33 nm), H2 (0.290 nm) and He (0.260 nm). The values correspond to the average of permeation data performed at different temperatures from 40 ^{o}C to 120 ^{o}C (lines were added for readability).

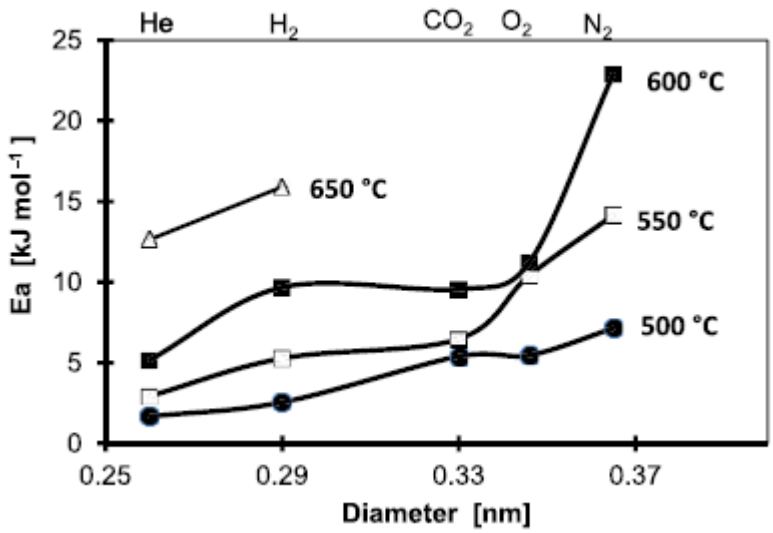

Fig. 13 - Activation energy for permeating species N2, O2, CO2, H2 and He in c-CMSM500-5m, c-CMSM550-5m, c- CMSM600-5m and c-CMSM650-5m membranes activated at 200 ^{o}C under N2 (lines were added for readability)

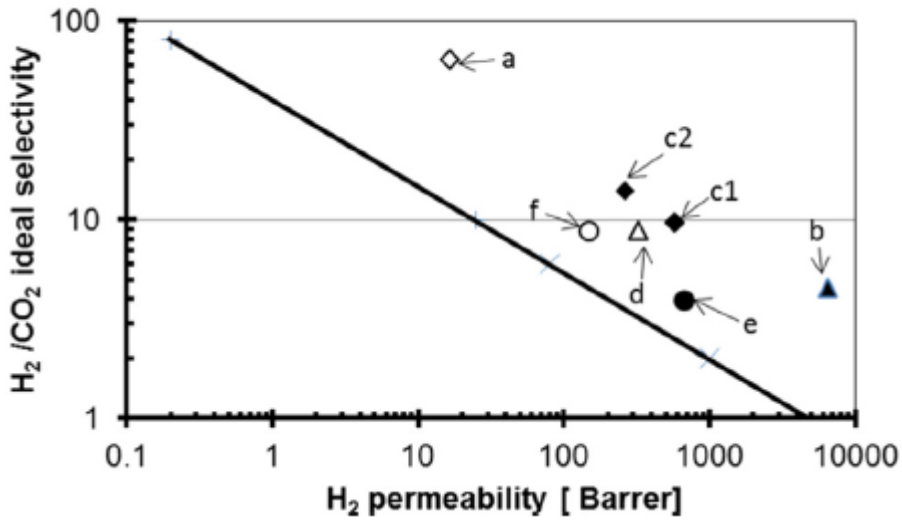

Fig. 14 e Robeson's revised upper bound for H2/CO2 and values from the literature and from this work for carbon molecular sieve membranes: (a) Low [80], (b) Bux [81], (c1) this work (CMSM600-200-80), (c2) this work (CMSM600-200-30), (d) Hosseini [61], (e) Mc Carthy [82], (f) Campo [52].

Table 1 – H_2 permeability and H_2/N_2 permselectivities for carbon molecular sieve membranes.

Precursor	Pyrolysis conditions	H_2 permeance barrer	Selectivity H_2/N_2	Reference
Kapton	600 °C, 120 min	1600	19.6	Suda & Haraya [59]
	800 °C, 120 min	669	220	
	1000 °C, 120 min	59.4	1450	
Polyfurfurylalcohol	300 °C, 120 min	0.83	175	Shiflett [60]
	450 °C, 120 min	3.63	331	
	600 °C, 120 min	8.14	29.8	
Polypyrrolone	500 °C, 60 min	6580	88.6	Kita et al., [43]
	700 °C, 60 min	1720	267.5	
	800 °C, 60 min	25.4	1080.9	
PBI		0.60	125.1	Hosseini [61]
Matrimid		27.2	97.0	
PBI/Matrimid(50/50 wt%)	600 °C	1337	85.1	
PBI/Matrimid(50/50 wt%)	700 °C	940.3	149.3	
PBI/Matrimid(50/50 wt%)	800 °C	324	257.1	
Matrimid	650 °C	323	4.41	Briceño et al. [47]
CMSM from cellophane	550 °C, N_2	168.1	390	Campo et al. [52]
CMSM from Resol-phenolic resin	550 °C, N_2	2047	65.6	Texeira et al. [55]
CMSM from Resorcinol-formaldehyde resin	550 °C, N_2	301	>586	Rodrigues et al. [56]

Table 2 – Structural parameters of the c-CMSM carbonized at different temperatures.

Sample	I_D/I_G	f (%)
CMSM-500	0.536	34.9
CMSM-550	0.636	38.9
CMSM-600	0.658	40.1
CMSM-650	0.764	43.3
CMSM-700	0.768	43.4

Table 3 – Structural parameters determined from the DA fit for the c-CMSM carbonized at different temperatures.

Carbonizing end temperature °C	n	W_0 $cm^{-3}\,g^{-1}$	E_0 $kJ\,mol^{-1}$
450	2.14	0.119	11.6
550	2.30	0.131	12.2
650	2.75	0.167	14.1
750	2.29	0.192	11.8

Table 4 – c-CMSM permeances at room temperature to O_2, and N_2 and ideal permselectivities after carbonization (fresh membranes) at various temperatures.

Temp °C		mol m^{-2} s^{-1} Pa^{-1} × 10^{-9}			Temp °C		mol m^{-2} s^{-1} Pa^{-1} × 10^{-9}		
		N_2	O_2	O_2/N_2			N_2	O_2	O_2/N_2
CMSM450-F	450	4.9	10	2.1	CMSM700-F	700	94	175	1.9
CMSM500-F	500	72	121	1.7	CMSM750-F	750	22	88	4.0
CMSM550-F	550	140	198	1.4	CMSM800-F	800	31	10	0.3
CMSM600-F	600	136	209	1.5	CMSM850-F	850	16	6.8	0.4
CMSM650-F	650	157	296	1.9	CMSM1000-F	1000	27	9.5	0.4

Table 5 – c-CMSM permeance to N_2, O_2, H_2 and He at 30 °C and ideal permselectivities for c-CMSM carbonized at different temperatures after 1 day aging.

	mol m^{-2} s^{-1} Pa^{-1} × 10^{-9}				Ideal permselectivity		
	N_2	O_2	H_2	He	O_2/N_2	H_2/N_2	He/N_2
CMSM450-1d	0.4	1.0	19.7	8.2	2.5	49	2.4
CMSM500-1d	1.2	8.5	140.0	58.2	7.1	117	2.4
CMSM550-1d	0.2	3.0	145.0	79.5	15	725	1.8
CMSM600-1d	n.d	n.d	18.9	14.4	–	–	1.3
CMSM650-1d	n.d	n.d	5.6	2.1	–	–	2.7
CMSM750-1d	n.d	n.d	5.1	1.2	–	–	4.3

n.d. below detection limit <8 × 10^{-11} mol m^{-2} s^{-1} Pa^{-1}.

Table 6 – Activation energy for permeating species N_2, O_2, CO_2, H_2 and He at 30 °C in c-CMSM500-5m membrane after 20 weeks of aging and upon activation at various temperatures.

	Diameter (nm)	E_a (kJ mol^{-1})[a]					
		100 °C	120 °C	140 °C	160 °C	180 °C	200 °C
N_2	0.365	19.8	16.8	11.7	13.8	7.2	7.2
O_2	0.346	16.7	12.0	10.5	12.3	5.5	5.5
CO_2	0.335	22.7	18.1	12.4	13.2	5.4	5.4
H_2	0.290	8.3	5.7	5.1	5.5	2.5	2.5
He	0.260	4.0	3.2	2.5	2.9	1.5	1.5

[a] E_a calculated using eq. (4).

Table 7 – Activation energy for permeating species N_2, O_2, CO_2, H_2 and He at 40–120 °C in c-CMSM500-5m, c-CMSM550-5m, c-CMSM600-5m and c-CMSM650-5m membranes, activated at 200 °C under N_2.

	Diameter (nm)	E_a (kJ mol^{-1})[a]			
		500 °C	550 °C	600 °C	650 °C
N_2	0.365	7.1	14.1	22.9	n.d.
O_2	0.346	5.5	10.4	11.2	n.d.
CO_2	0.335	5.4	6.5	9.6	n.d.
H_2	0.290	2.6	5.3	6.7	15.9
He	0.260	1.7	2.9	5.2	12.6

n.d. (permeance below the detection limits).
[a] E_a calculated using eq. (4).